

promoting access to White Rose research papers



Universities of Leeds, Sheffield and York
<http://eprints.whiterose.ac.uk/>

This is the author's pre-print version of an article published in the **IEEE Sensors Journal**

White Rose Research Online URL for this paper:

<http://eprints.whiterose.ac.uk/id/eprint/76053>

Published article:

Hobby, MJ, Thomas, RE, Gascoyne, M, Parsons, DR, Keevil, GM, Peakall, J and Carrivick, JL (2013) *MEMS-integrated load cell for measuring pressure, erosion, and deposition in dynamic environmental flows*. IEEE Sensors Journal, 13 (2). 492 - 500. ISSN 1530-437X

<http://dx.doi.org/10.1109/JSEN.2012.2217953>

A MEMS Integrated Load Cell (MILC) for measuring pressure, erosion & deposition in dynamic environmental flows

M J Hobby, R E Thomas, M Gascoyne, D R Parsons, G M Keevil, J Peakall, J Carrivick

Abstract—A MEMS Micro Electro-Mechanical System-based load cell has been integrated with signal conditioning circuitry, temperature and tilt sensors for measurement of sediment-fluid interaction and flow under turbulent conditions. Such an instrument is of great value for improving understanding of quantifying turbulent flow and sediment dynamics within flood events and river or coastal erosion settings, for example. Sensor sensitivity was tested to a mass of 0.5g but can be shown theoretically to extend to 50mg. The sensor was found to have no attenuation of frequencies up to 2.5Hz and would therefore be suitable for monitoring turbulent flow. Laboratory flume experiments, simulating a dam burst, demonstrate the applicability of the sensor for measuring highly dynamic and transient flow phenomena in unprecedented detail.

Index Terms—MEMS, flood, erosion, flow, load cell, environmental monitoring

I. INTRODUCTION

MEASURING turbulent flow properties such as dynamic fluid pressures, shear stresses, and the associated erosion, transport and deposition of particles at the fluid-sediment interface is of paramount importance for advancing our knowledge of a range of complex environmental flows, such as including those that occur during avalanches, debris flows, floods or longer-term and/or larger-scale events [Error: Reference source not found, [6], [5][7], [8][8]]. However, successful monitoring of such spatially-distributed processes over the range of relevant temporal scales is notoriously difficult. Existing laboratory-based techniques including acoustic [14] or laser [11] Doppler velocity probes, echosounders [2], terrestrial (ground-based) LiDAR and close-range photogrammetry [3] generally capture only either spatial or temporal variability and have to neglect the other dimension. This focus on a single dimension can introduce significant uncertainties when attempting to quantify fundamental processes in systems that exhibit coincident and/or concurrent spatio-temporal changes. In addition, the pressure field and/or the shear stress exerted at the flow-sediment interface has often only been estimated through extrapolation of *in situ* velocity measurements [5], and to date, pressure transducers or electrical conductivity probes [12][13] have only captured gross bed-sediment transport rates [1] or pressures on static concrete slabs [12].

Recent advances in Micro Electro-Mechanical Systems

(MEMS) now enable the construction of load cell arrays at the laboratory scale with potential to measure the dynamic pressures induced by turbulent flow and sediment transport processes. Herein, we present the aim of this paper is to present the development and initial application of a single MEMS Integrated Load Cell (MILC). MEMS load cell-based laboratory device. The MILC that has is been integrated with an accelerometer and a thermistor, to make supporting observations of sensor orientation and temperature, respectively, and was combined with low noise signal conditioning electronics and enclosed within a small-footprint instrument housing. This In order to demonstrate the design of the device is and its capability capable of obtaining very detailed spatio-temporal process information at the sediment-flow interface. The instrument has been termed the MEMS Integrated Load Cell (MILC). In the present paper, we herein: first i) outline the design of the instrumentation. Second, we, ii) describe initial tests and calibration. Third, we, iii) demonstrate the quality and validity of laboratory flume data obtained using the device. Finally, we, iv) outline potential extensions of the design and suggest avenues for deployment that will help improve our substantive understanding of geophysical flows.

II. INSTRUMENT OVERVIEW

The rationale behind the scientific specification of a sensitive and accurate pressure sensor device for laboratory application mainly concerns the desires absolutely necessary for for the quantification of the smallest spatio-temporal resolution of pressure measurements while whilst still allowing the broadest possible application range. To enable the detection of turbulence-induced fluctuations of pressure, the an instrument must be capable of measuring pressure variations < 1 Pa active over a spatial extent < 2000 mm² and at a sampling rate > 20 Hz. In most environmental fluid dynamics laboratories, the maximum operating depth of water is of the order of 1m and therefore, the instrument must also be capable of measuring maximum static loadings of ~9810 Pa. Finally, the instrument must be rugged, resistant against impact and abrasion and capable of operating reliably over a range of temperature conditions in electrically 'noisy' environments.

A. Principle of Operation

The laboratory instrument described herein measures the

Comment [JLC1]: Personally I think that the use of acronyms in titles is to be avoided.

Comment [JLC2]: Is this symbol used/permitted in the target journal? I would have thought that 'and' would be more appropriate.

Comment [JLC3]: I do not know what this acronym is, which is not helpful because the abstract should 'stand-alone'. I have inserted the full definition

Comment [JLC4]: Is it correct for the target journal to list references alphabetically, because this results in these citation numbers being out of sequence in the manuscript? i.e. I would expect number 1 to be first!

Comment [JLC5]: Rather vague...can we quantify what short time-scales we are talking about?

weight of a column of fluid and/or sediment directly above a MEMS load cell. The load cell itself measures the force acting upon a plate of fixed area. The measured load is thus directly proportional to the pressure.

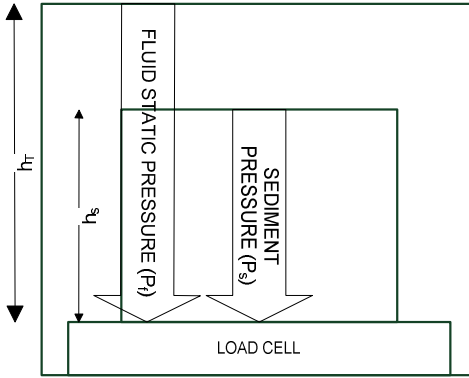


Fig. 1 - Measurement principle behind the MEMS Integrated Load Cell (MILC), demonstrating the combined measurement of fluid and sediment

Within the context of an experimental flume facility, the total pressure measured by the load cell, P_T , has two components: the pressure due to the sediment (if any) within the flume, P_s , and the pressure due to the fluid, P_f (Fig. 1 Fig. 4):

$$P_T = P_s + P_f$$

Note that the term “fluid” does not differentiate between purely clear-water flow and water containing a finite amount of suspended matter.

P_s is dependent on the thickness of sediment within the column (h_s), the saturated bulk density of that sediment (ρ_s) and the gravitational constant (g):

$$P_s = h_s \rho_s g$$

Similarly, P_f is dependent on the total height of the column (h_T) and the fluid density (ρ_f):

$$P_f = (h_T - h_s) \rho_f g$$

Assuming no instantaneous change in the water surface elevation, when sediment is eroded the volume of sediment in the measurement column reduces and the volume of water increases by an equal amount. Conversely, as sediment is deposited, the volume of water in the measurement column reduces and the volume of sediment increases by an equal amount. Defining the change in the thickness of sediment, Δh , as positive for erosion and negative for deposition, the change in pressure, ΔP , caused by Δh can therefore be described by:

$$\Delta P = g \rho_f \Delta h - g \rho_s \Delta h = g (\rho_f - \rho_s) \Delta h$$

Dynamic variations in pressure can thus be measured and the thickness of sediment inferred.

B. Electronic System Design

The system is based around a Honeywell FSS series load cell,

which was chosen due to its low drift properties. The Honeywell FSS series uses piezo-resistors in a Wheatstone bridge configuration. The piezo-resistors are machined from silicon and actuated directly by a stainless steel ball. The nominal resistance of the bridge was measured to be $4.6k\Omega$. The differential bridge output is reported to range from $0.12mVg^{-1}$ to $14mVg^{-1}$ and therefore needs to be amplified before digital conversion (Fig. 2 Fig. 2).

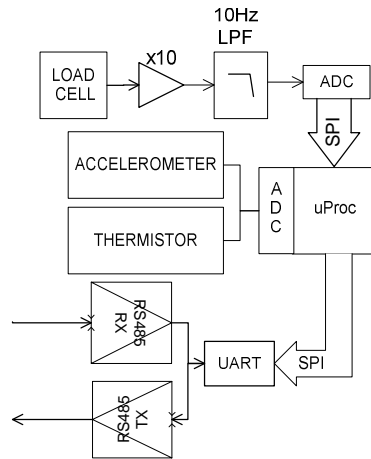


Fig. 2 – Schematic block diagram of the MILC

The differential signal from the load cell is amplified using an instrument amplifier. The gain of the amplifier is set to 25.7 using standard value resistors with a low temperature coefficient, maintaining consistent gain across the temperature range. The gain is set to maximize sensitivity while ensuring the amplifier is not saturated prior to the load cell reaching its maximum load.

A simple low-pass (LP) filter is used to minimize aliasing distortion and maximize signal-to-noise ratio. The breakpoint of the filter is set to $\sim 160Hz$, so as to be above any frequency of interest. Precision components were not used in the filter since the breakpoint was chosen relatively arbitrarily.

To ensure the ADC input was not overloaded (which would cause fatal damage to the ADC), a Schottky diode clamp to the digital positive rail (+5V) was used. Maximum linear headroom was achieved by using a diode with a low ‘turn-on’ voltage. The load cell and ADC are both fed by precision voltage references, which can be adjusted using preset resistors during the calibration process.

Two additional sensors have been incorporated within the design. First, a MEMSIC dual-axis accelerometer, the axes of which are aligned with the horizontal, is included to enable the MILC instrument to be oriented at angles other than normal to the gravitational field vector. This accelerometer was selected because of its small form factor, requiring less circuit board space. Second, a Betatherm thermistor bead has been placed as

close to the load cell as possible to allow account to be taken of changes in the mechanical response of the load cell with changes in temperature.

Internal peripheral communication is carried out using a Serial Peripheral Interface (SPI) bus. SPI bus master and instrument control is carried out on an Atmel ATmega644 microcontroller, which has an embedded 10-bit ADC. This was considered suitable for the temperature measurement and accelerometer tilt measurements but a higher degree of accuracy was required for the load cell. Therefore, an ADI AD7680 ADC was used, due to its availability in a small form factor (SOT-23 package). The Effective Number of Bits (ENOB) of this device is ~13.83.

The circuit design was split across two circuit boards: the analog signal conditioning and the digital processing. This was done to minimize noise and interference from the high speed switching of digital communication lines. The ADC was placed on the analog signal conditioning board, which communicated with the digital board using SPI. Special care was taken to minimize the effects of interference from this source by careful routing of digital signal return paths. Analog and digital grounds were kept apart and linked at one point, close to the power input. The dual-deck circuit boards are shown in Fig. 3.

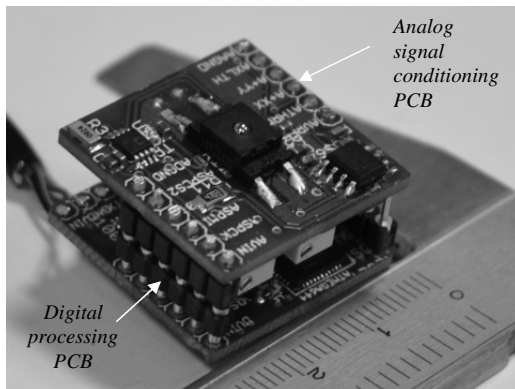


Fig. 3 – Dual-deck approach to the circuit design to minimize noise and interference from high speed digital communication lines. The scale is in centimeters.

An array of MILCs is required to make spatially-distributed measurements of pressure, and thus turbulent velocity fluctuations, and/or erosion and deposition of sediment. Data from each MILC must be synchronized to other units in the array. A real-time data logger is therefore used to gather data from the array, with individual MILCs attached to a RS485 bus. MILC units are addressed individually in software using a node ID. When not driving the bus, the MILC driver switches to high impedance, freeing the line for other instruments in the array.

A 'DataLink' layer was defined to sit above the 'Physical'

layer provided by the RS485 standard as shown in

Fig. 4. Communication is initiated with a 'start' bit sequence followed by 5 bits for the actual command. The second byte is always the node ID. An ID of 0 indicates a broadcast command. All instruments in the array are instructed to perform a measurement using a broadcast command with data being subsequently collected by a specific addressed command.

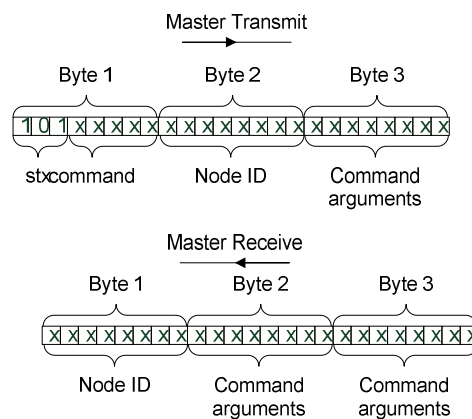


Fig. 4 –Data communication packet structure used in MILC 'DataLink' layer

C. Mechanical Design

The MILC is presently housed inside a 29mm radius cylindrical shell that is split into five sections (Fig. 5). Particular attention is drawn to the rubber diaphragm, which is clamped in place by the top flange and forms a watertight seal with the main shell. This diaphragm provides the contact between the fluid outside the instrument and the load cell. To maximize sensitivity to load variations, brass plates are affixed to the top and bottom of the center of the diaphragm to locally increase its stiffness. The edges of the diaphragm are free to move so that changes in load above the top plate are transmitted as faithfully and quickly as possible to the load cell.

The circuit boards fit snugly inside the outer housing, but a screw fed from the bottom of the instrument prevents any slack in the system. In addition, because this screw drives the circuit board, and therefore the load cell, into the diaphragm it can also be used to manually tare the instrument and ensure that the load cell is within its linear operational range. The screw head is covered by a cap which is sealed with an O-ring. Cabling feeds through the bottom flange and watertight seal. An O-ring is used to seal the bottom flange to the main shell, with six screws clamping it in place. The top flange, main shell and bottom flange are presently constructed of brass, owing to its availability, strength and resistance against abrasion within harsh laboratory conditions. This shell has been tested in up to 1m deep water with no signs of water ingress. Modern polymers are an attractive alternative to brass because they provide similar strength properties, significant material cost

Formatted: Default Paragraph Font

savings and permit rapid mass-manufacture using injection-molding processes.

III. TESTING THE ANALOG CIRCUITRY DESIGN

A series of tests were conducted to ensure that the amplitude response of the system was linear, the frequency response was above 20Hz and noise was minimal. Two different methodologies were adopted. First, the signal conditioning circuitry was modeled in SPICE software (National Instruments MultiSim) to simulate the amplitude response, frequency responses and output noise. The load cell was modeled as a Wheatstone bridge with all resistances set to 4.6k Ω . Precision voltage references were modeled as perfect voltage sources in series with a thermal noise source producing the same level of noise as quoted in the component datasheets, and the amplifier was modeled using the SPICE model supplied by its manufacturer. Second, physical tests were conducted on a prototype, as per the final 'dual deck' design, to identify amplitude response and output noise. During these tests, the load cell was removed from the circuit board and simulated using a Wheatstone bridge of 4.6k Ω resistors. One resistor in the bridge was replaced with a variable resistor to adjust the output of the bridge.

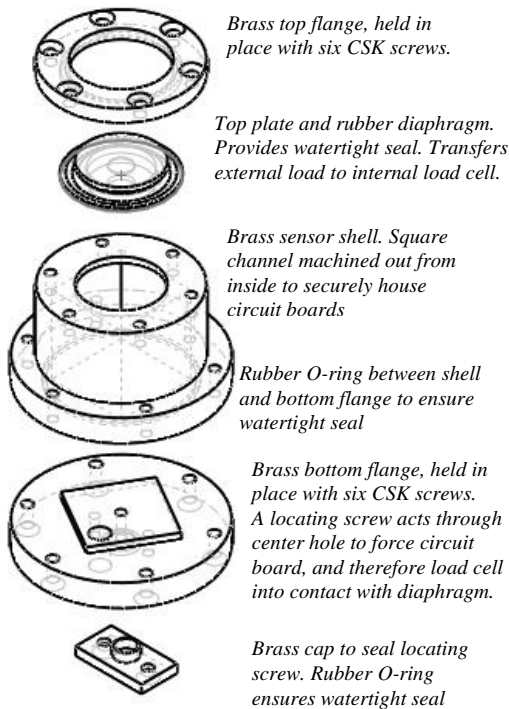


Fig. 5 – Schematic of mechanical layout of the MILC

A. Amplitude Response

Both testing methodologies were employed to study the amplitude response of the load cell signal conditioning circuitry. Using the first 'modeling' method, the output of the load cell was monitored as the resistance of one resistor in the bridge was adjusted. These tests clearly identified the linear region of the amplifier between 'floor' and 'ceiling' points at ~0.7V and 5.1V, respectively (Fig. 6 – 'circles'). The clamping diode did not cause any degradation of linearity up to 5V (maximum possible input value of ADC).

The second 'prototype' method demonstrates the same linear response, extending slightly lower (Fig. 6 – 'crosses').

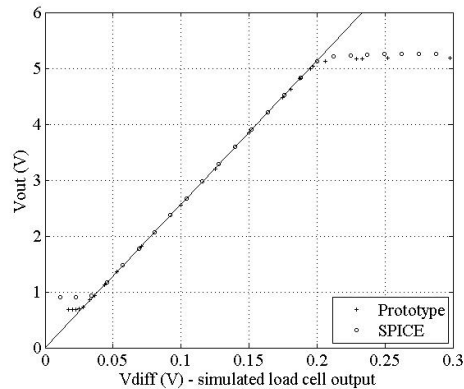


Fig. 6 – Modeled (o) and prototyped (+) analog signal conditioning electronic circuitry demonstrating the linear operation, within limits, of the MILC front end. The input load cell was simulated using resistors in a Wheatstone bridge configuration.

B. Frequency Response

To study the frequency response of the instrument, the modeling method was used. An AC source was placed in series with the Wheatstone bridge, with one resistor set slightly lower than the others to produce a DC offset. The AC source was swept from 0.1Hz to 500Hz. The simulated amplitude and phase response are shown in Fig. 7, demonstrating flat response in excess of 20Hz.

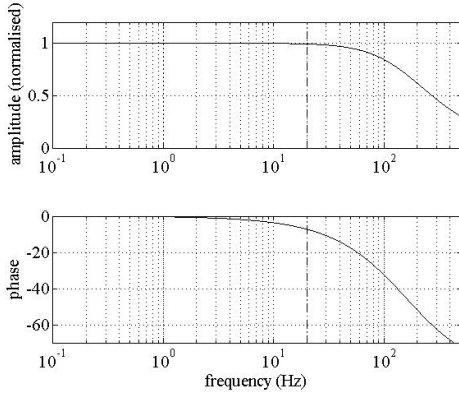


Fig. 7 – Modeled normalized frequency response of analog signal conditioning circuitry, demonstrating flat response up to 20Hz (indicated vertical by the dashed line).

C. Noise

Both testing methodologies were employed to study the noise introduced by the signal conditioning circuitry. The noise was investigated at the point the signal conditioning circuit connects to the ADC. The model predicted a total output noise of $33.3\mu\text{V}$ rms. Conversely, 25,000 measurements of voltage (taken at 1Hz) made from the prototype yielded a total output noise of $650\mu\text{V}$ rms. The difference is thought to be due to an oversimplification in the model.

IV. CALIBRATION & TESTING

A. Calibration- Load against Voltage

To calibrate the MILC, a range of calibrated weights (500g, 200g, 100g, 50g, 20g, 10g, 5g, 2g, 1g, and 0.5g, equivalent to pressures of $\sim 9680\text{Pa}$, $\sim 3870\text{Pa}$, $\sim 1940\text{Pa}$, $\sim 968\text{Pa}$, $\sim 387\text{Pa}$, $\sim 194\text{Pa}$ and $\sim 96.8\text{Pa}$, respectively) were placed on the MILC and ~ 700 data points were collected at a frequency of 100Hz. The adjustment screw was tightened until the MILC output increased above 0.7V, demonstrating that the load cell was in contact with the diaphragm and the unit was operating in its linear region. Data was averaged across all the points for each load and plotted against the applied load (Fig. 8). Linear regression yielded coefficients of determination, R^2 , close to 1.0 for all instruments tested. Small loads caused a greater spread about the linear fit. This is due to the decreased load not displacing the brass plate of the instrument to as large a degree as greater load. Further tests were carried out using a fixed load to bias the instrument and then adding smaller loads. The coefficients for each individual MILC varied slightly, with an average slope of 151gV^{-1} ($\pm 6\text{gV}^{-1}$) and offset of -171g . The variation in slope is due to the tolerance in component values and remains fixed for an individual MILC system. The variation in offset is caused by the adjustment screw, which is used to ensure the unit is operating within the linear region of response, and can be adjusted between experiments. The data obtained in this test can be extrapolated

to infer a maximum load of 584g at 5V. Using the known surface area of the top plate (506.7mm^2), the density of water at 10°C (999.7kgm^{-3}) and the gravitational acceleration (9.807ms^{-2}), this MILC unit is therefore capable of measuring pressures in water columns up to 1.15m deep. The adjustment screw could be loosened to obtain a greater range, at the risk of operating outside the linear region for small weights. Greater range can also be achieved by decreasing the amplifier gain, which in turn decreases resolution.

A. Calibration- Voltage against Temperature

As noted previously, it is known that the mechanical response of load cells is temperature-dependent, thus necessitating the inclusion of a temperature sensor to calibrate the system. To characterize this changing response and thus quantify the calibration required, the MILC was first placed in an ice bath to decrease its temperature. The instrument was then removed and both output voltage and temperature were logged as the instrument warmed to room temperature. The unit was then heated to 50°C . Output voltage and temperature were logged as the instrument subsequently cooled to room temperature. Raw load and temperature data from both experiments were concatenated and filtered using an 8-point moving-average filter, to minimize random noise in voltage and temperature signals.

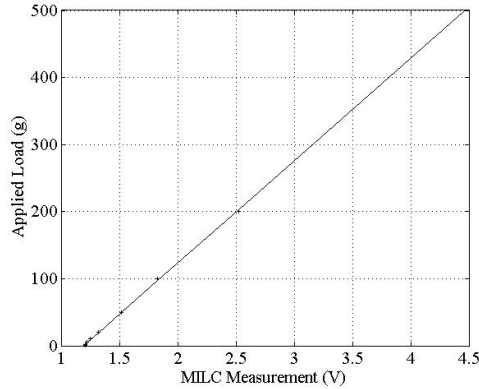


Fig. 8 – Applied static load (in grams) against MILC measurements (in Volts).

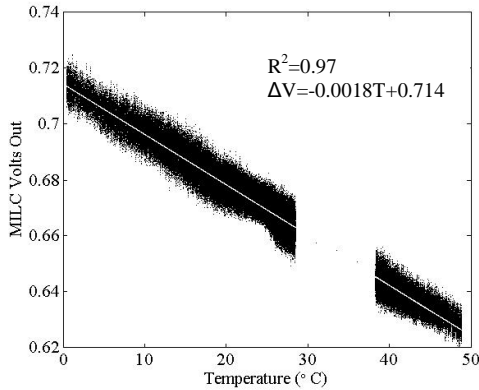


Fig. 9 – Variation in MILC output with varying temperature. The linear best fit line is shown as the white line. Data was gathered from two experiments where the MILC was allowed to return to room temperature from either operational temperature extremes. Limited data was obtained between approximately 28°C and 38°C.

Linear regression characterized the relationship between temperature, T , and change in measured voltage, ΔV , as (white line; Fig. 9):

$$\Delta V = -0.0018T + 0.714$$

The coefficient of determination for this fit (R^2) is 0.97.

B. Noise

The total system noise, ε_T , is given by:

$$\varepsilon_T^2 = \varepsilon_i^2 + \varepsilon_q^2$$

where ε_i is the noise at the input to the ADC (650 μ V rms; §III C) and ε_q is the root mean square error in the ADC, given by [9] as:

$$\varepsilon_q = \frac{V_{fs}}{2^{ENOB}} 12^{-1/2}$$

where V_{fs} is the full range of the ADC (5.0V) and ENOB is the Effective Number Of Bits, which can be calculated from the information within the datasheet to obtain ~ 13.83 [10][9]. ε_q is therefore found to be 99.1 μ V rms and ε_T is 658 μ V rms.

Following calibration, it is known that the load cell output changes by $\sim 330\mu$ V for a 50mg change in applied load (~ 0.97 Pa change in pressure). Thus, noise is the limiting factor in the sensitivity of the MILC to pressure fluctuations. To observe the required voltage levels below the level of noise, the noise must be diminished through oversampling. This has the additional benefit of increasing the ENOB and hence increasing the resolution. Oversampling has therefore been implemented onboard the MILC instrument, invisible to the user, producing a single average result based on a number of samples. Oversampling onboard the MILC instrument has the advantage that RS485 traffic is minimized. Conversely, oversampling onboard has the disadvantage that the MILC becomes unresponsive for the time to take a single sample ($\sim 2.5\mu$ s) multiplied by the oversampling factor.

The oversampling factor invoked by the MILC can be set to

a power of 2, from 2^0 up to 2^{10} (1024), so as to enable division via a simple bit shift. Total noise diminishes as:

$$\varepsilon_T(N) = \frac{1}{\sqrt{N}} \varepsilon_T(0)$$

where $\varepsilon_T(N)$ is the total noise with an oversampling factor of N and $\varepsilon_T(0)$ is the total noise with no oversampling. Thus, with the oversample factor set to 64 (2^6), the noise diminishes to 82 μ V rms, equivalent to ~ 12 mg change in load (~ 0.23 Pa change in pressure). Using the maximum oversample factor of 1024, the noise can be further reduced to 20.5 μ V rms. With these levels of electronic noise, the response of the instrument is dominated by the mechanical structure of the shell. However, since the return packet data is limited to 2 bytes the ENOB cannot be greater than 16, equivalent to an oversample factor of 20.25. This is achieved by the MILC with an oversample factor of 32 (2^5) [10].

Further increase of temporal resolution can be obtained by requesting more samples from the MILC within a given time period. However, this results in a compromise on the overall data throughput, which is dependent on the maximum frequency of data required or the number of MILC instruments on any single RS485 bus.

C. Frequency Response

To quantify frequency response of the MILC, the instrument was placed at the bottom of a graduated cylinder with an internal diameter of 73mm and a peristaltic pump was used to first fill and then empty the cylinder at various rates. The pump outlet was clamped a few millimeters above the center of the top plate of the MILC in order to limit tube motion that might induce water motion in the cylinder and therefore periodically disturb the water surface.

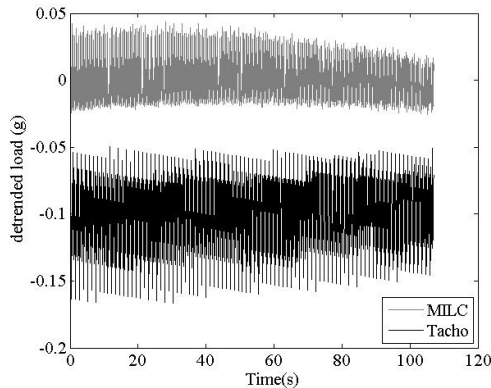


Fig. 10 Time series data, showing the MILC and pump tachometer data while the pump output is directed towards the top plate of the MILC.

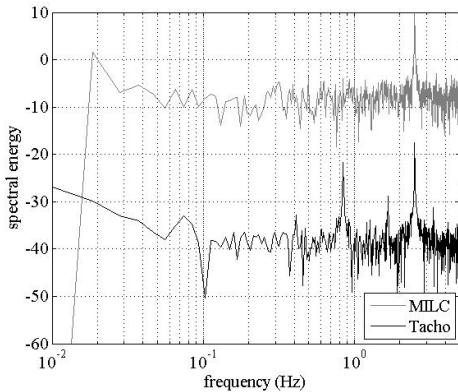


Fig. 11 – Comparison of data in the frequency domain between the MILC instrument and a peristaltic pump delivering pulses of water onto the top plate of the MILC at a rate of 2.5Hz. Tachometer data is offset in the y-axis to enable clearer comparison.

The Watson-Marlow peristaltic pump employed herein is readied for use by clamping specially-manufactured silicon tubing full of water inside a circular pump casing. As a cam shaft fitted with three rollers rotates at a user-configurable rate (in revolutions per minute), the tubing is compressed against the casing and water is forced to move through the tubing. Thus, by setting the revolution rate to 50rpm, the three ‘doses’ that are outputted per pump shaft revolution yielded a dosage frequency of 2.5Hz. A digital tachometer on the cam shaft that produces 343 pulses for every revolution was used to monitor the fractional rotation of the shaft. To enable comparison of data from the MILC and the tachometer, their outputs were logged synchronously with a National Instruments Compact RIO real time logging computer. The voltage-temperature calibration of the unit (§IVB) was applied to the MILC data, and then the data from a single fill cycle were linearly de-trended to remove the overall trend of increasing load. As the cylinder filled, the magnitude of the load fluctuations detected by the MILC diminished over time (Fig. 10), as the pressure imposed by each dose of water became a smaller and smaller fraction of the total hydrostatic pressure of the water in the cylinder.

To identify and compare the main system harmonics, both datasets were subjected to a Fast Fourier Transform (Fig. 11). Note that the tachometer data has been offset on the y-axis to facilitate comparison. The 2.5Hz fundamental can be clearly seen in both the tachometer and MILC outputs, with no decrease in amplitude (Fig. 11). Although this test cannot prove that the MILC responds at its target specification (20Hz) owing to limitations of the peristaltic pump, it is not unreasonable to expect to be able to monitor turbulent load/pressure fluctuations within the frequency measurements made. Needless to say, variations will be averaged across the vertical column. There are two further sub-harmonics at lower frequencies in the tachometer data that are not apparent in the

MILC data. These are hypothesized to be due to the pump tachometer processing and do not represent real oscillations in the cylinder.

V. INITIAL RESULTS

With MILC system characteristics fully quantified, the system was deployed and tested during flume experiments conducted at the Sorby Environmental Fluid Dynamics Laboratory (SEFDL) at the University of Leeds. Following [4][5], a simple dam-break set-up was constructed within a $4.0 \times 0.2 \times 0.5\text{m}$ ($l \times w \times d$) flume. Four MILC units were installed at downstream distances of 1.5 and 2.5m from the ~~a~~ dam-break-release-lock gate. The MILC units were positioned at cross-stream distances of 0.05 and 0.15m, respectively. To initiate dam break outburst floods, a gated lock-box was filled to a depth of 0.5m with clear water. The lock gate was then raised instantaneously by 80mm, permitting water to flow out from below the raised gate and across the flume floor that was uniformly covered in ~75mm of mobile fine gravel (median grain size, $D_{50} = 5\text{mm}$; [4]). At each downstream distance, one MILC unit was covered by a porous cap that permitted loading only by water, while the other was loaded by both water and gravel. Each experimental run lasted for ~30s. Flow depth/head variations throughout the flood wave were recorded by the instruments. Flows were also monitored through the flume wall with side-looking high-speed 50fps video cameras. The results show the performance of the MILCs in relation to the depths calculated using the video camera records.

Fig. 12 shows the temporal variation of the total flow depth (h_T) or stage and the associated temporal variation of the relative pressure measured by the MILCs (note that the hydrostatic pressure has a component due to the water and the sediment in the sediment+water case). As the flood front arrives, relative pressure rapidly falls to less than hydrostatic in both the water only and sediment+water cases, before slowly recovering to (near) hydrostatic from ~3-4 s after the release of the lock gate. This rise is commensurate with the gradual decrease in water depths and flow velocities following passage of the flood peak. The delay between flood peak arrival at 1.5m and 2.5m is clearly observed.

Comment [JLC6]: Should this be [4]?

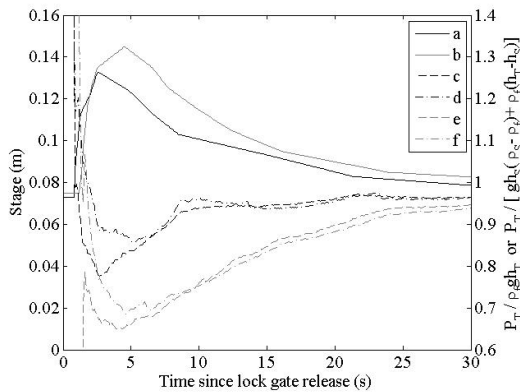


Fig. 12 – Temporal evolution of the stage (= total flow depth, h_T) at 1.5m (a) and 2.5m (b) downstream. The relative pressure of the outburst flood as it propagates across a bed of fine gravel is shown for both sediment and water at 1.5m (c) and 2.5m (e). Relative pressure for water only is shown at 1.5m (d) and 2.5m (f).

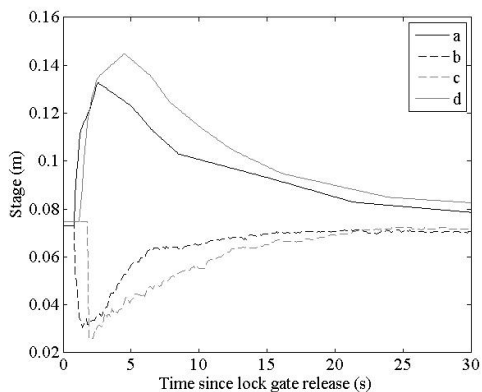


Fig. 13 – Temporal evolution of the stage (= total flow depth, h_T) of the outburst flood at 1.5m (a), 2.5m (b) downstream and the associated erosion as it propagated across a bed of fine gravel, again at 1.5m (c), 2.5m (d) downstream.

The inferred changes in bed elevation associated with the passage of the flood wave shown in Fig. 12 are highlighted in Fig. 13. 40-45mm of erosion is estimated to occur as the highly turbulent flood front passes the MILCs, with sediment transported from upstream almost completely in-filling the sediment bed following passage of the flood front. Net erosion is estimated to be 1-3mm. However, ~~while~~ ~~whilst~~ our observations suggest that the latter estimate is realistic, the maximum scour depths do not appear to be so. We hypothesize that this is either caused by changes in the porosity of the sediment bed, causing (unmeasured) changes in its bulk density or more likely to the generation of a quasi-suction effect during the passage of the highly turbulent flood wave, reducing pressures to less than hydrostatic. ~~The latter~~

hypothesis is supported by pressure measurements on immobile beds.

VI. SUMMARY

This paper has presented the development and testing of a novel MEMS based sensor capable of recording micro-scale pressure variations in geophysical flows in a laboratory setting. The linearity, noise and frequency response have been quantified and found to be within, or close to the initial specification. In its current form, the MILC has been shown to be capable of recording the depth/head variation of a dam-break outburst flood flow at high temporal resolution and to a high degree of accuracy. ~~It~~

The development and application of MEMS load cells is of particular importance since the reduced (and, with continuing technological advances, reducing) size of such sensors could potentially increase the spatial resolution of measurements to the order of 1mm while retaining their temporal resolution (>100Hz). Both of these specifications improve upon presently available technologies such as X and X. The largest physical element of any MEMS sensor tends to be the housing that enables integration with other components. The successful demonstration of a single MEMS sensor to measure particulate flows is an important step towards realizing many load cells on a single silicon substrate for example. The further extension of the present work from single sensors to large arrays of sensors holds significant promise for enabling improved understanding of the most complex geophysical and sedimentological flows.

We therefore consider that MILCs has have significant potential for examining sediment transport processes and quantifying the spatio-temporal extent of erosion and deposition induced by a range of geophysical flows. Its-The relatively low power of operation (less than 0.5W), together with its rugged, waterproof housing, means that iMILCs t-also lends itself will also be suitable to-for long-term field installations as well as the laboratory applications similar to those presented herein. The A MILC may-could also be used to examine other types of particulate flows and capture the dynamics of bedform migration in sands and/or gravels, examine the detailed dynamics of turbidity driven currents, or indeed examine snow avalanches and/or the impact of raindrops/hailstones on the Earth's surface.

The development and application of MEMS load cells is of particular importance since the reduced (and, with continuing technological advances, reducing) size of such sensors could potentially increase the spatial resolution of measurements to the order of 1mm while retaining their temporal resolution (>100Hz). Both of these specifications improve upon presently available technologies. The largest physical element of any MEMS sensor tends to be the housing that enables integration with other components. The successful demonstration of a single MEMS sensor to measure particulate flows is an important step towards realizing many load cells on a single silicon substrate for example. The further extension of the present work from single sensors to large arrays of sensors

Comment [JLC7]: Our measurements? Or someone elses?

Formatted: Indent: First line: 0.36 cm

Comment [JLC8]: Plus it is virtually non-invasive, compared to other methods?

Comment [JLC9]: This paragraph is a bit rambling, and specific to the design of the MILC... I would trim it down and I have moved it upwards to place it first in this summary section, so as to finish with the most hard-hitting real-world application stuff...

Comment [JLC10]: A bit random...not part of the 'geophysical flows' type phenomena spoken about earlier... I suggest delete...

Comment [JLC11]: Plus it is virtually non-invasive, compared to other methods?

holds significant promise for enabling improved understanding of the most complex geophysical and sedimentological flows.

REFERENCES

- [1] Bergman, N., Laronne, J. B. and Reid, I., "Benefits of design modifications to the Birkbeck bedload sampler illustrated by flash-floods in an ephemeral gravel-bed channel." in *Earth Surface Processes and Landforms*, 32: 317-328, 2007.
- [2] Best, J. L. and Ashworth, P. J., "A high-resolution ultrasonic bed profiler for use in laboratory flumes." in *Journal of Sedimentary Research A*, 64: 674-675, 1994.
- [3] Butler, J. B., Lane, S. N., Chandler, J. H. and Porfiri, E., "Through-water close range digital photogrammetry in flume and field environments." in *Photogrammetric Record*, 17(99): 419-439, 2002.
- [4] Carrivick, J. L., Jones, R. and Keevil, G., "Experimental insights on geomorphological processes within dam break outburst floods." in *Journal of Hydrology*, 408: 153-163, doi:10.1016/j.jhydrol.2011.07.037, 2011.
- [5] Cossu, R. and Wells, M.G., "A comparison of the shear stress distribution in the bottom boundary layer of experimental density and turbidity currents." in *European Journal of Mechanics B / Fluids*, 32: 70-79, 2012.
- [6] Ernst, G. G. J., Sparks, R. S. J., Carey, S. N. and Bursik, M. I., "Sedimentation from turbulent jets and plumes." in *Journal of Geophysical Research*, 101(B3): 5575-5589, 1996.
- [7] Felix, M., Sturton, S. and Peakall, J., "Combined measurements of velocity and concentration in experimental turbidity currents." in *Sedimentary Geology*, 179: 31-47, 2005.
- [8] Garcia M. H., "Depositional turbidity currents laden with poorly sorted sediment." in *Journal of Hydraulic Engineering, ASCE*, 120(11): 1240-1263, 1994.
- [9] Glover I. and Grant M., "Digital Communications." Prentice Hall, 1024 pp, 2009.
- [10] Kest, W., "ADC Input Noise: The good, the bad, and the ugly. Is no noise good noise?" in *Analogue Dialogue*, 40-02, 2006.
- [11] Liu, Z., Adrian, R. J. and Hanratty, T. J., "Large-scale modes of turbulent channel flow: transport and structure." in *Journal of Fluid Mechanics*, 448: 53-80, 2001.
- [12] Melo, J.F., Pinheiro, A.N. and Ramos, C.N., "Forces on plunge pool slabs: Influence of joints location and width" in *Journal of Hydraulic Engineering, ASCE*, 132(1): 49-60, 2006.
- [13] de Rooij, F., Dalziel, S. B. and Linden P. F., "Electrical measurement of sediment layer thickness under suspension flows." in *Experiments in Fluids*, 26: 470-474, 1999.
- [14] Takeda, Y., "Instantaneous velocity profile measurement by ultrasonic Doppler method." in *Japan Society of Mechanical Engineers, International Journal Series B*, 35(1): 8-16, 1995.

Comment [JLC12]: This paragraph is a bit rambling, and specific to the design of the MILC...I would trim it down and place it first in this summary section, so as to finish with the real-world application stuff...